AERODYNAMIC STALL SUPPRESSION ON AEROFOIL SECTIONS USING PASSIVE AIR JET VORTEX GENERATORS

Simon A. Prince*, Vahik Khodagolian*, Chrisminder Singh*, Sunil Moir* and Anastasios Kokkalis**

***City University London, UK. ****CeBeNetwork Engineering & IT GmbH, Germany**

Abstract

This paper presents an experimental and computational study of a novel passive version of the air jet vortex generator flow control system for the delay or suppression of trailing edge boundary layer separation and subsequent stall. The results show that a passive vortex generating jet flow control system can effectively delaying trailing edge separation and subsequent stall to higher angles of attack, without the need for any active energy input and without significant drag penalty.

Nomenclature

α	Angle of attack (deg)
c	Chord length (m)
C_A	Axial force coefficient
C_D	Drag force coefficient
C_L	Lift force coefficient
C_M	$^1/_4$ chord pitching moment coefficient
C_μ	Blowing momentum coefficient
Cp	Pressure coefficient
$\dot{m}$	Mass flow rate through AJVG duct (kg/s)
p	Static Pressure (N/m^2)
p_0	Total Pressure (N/m^2)
ρ	Density (kg/m^3)
U	Velocity (m/s)
S	Reference (model planform) area (m^2)
x	Chordwise distance from leading-edge (m)
y	Spanwise distance from model centre (m)
z	Distance normal to the chordline (m)

Subscripts:

1	Local conditions
∞	Freestream conditions
j	Average conditions in jet at exit
t	Conditions at trailing edge

1 Introduction

Various flow control techniques, to reenergise boundary layers and thereby suppress flow separation, have been successfully tested, such as slot blowing, tangential blowing and synthetic jets. The method of increasing fluid mixing rates by the artificial generation of near surface longitudinal vortices has been found to be a particularly powerful technique. The vortices act to entrain high-energy flow from the undisturbed outer air stream and transport it into the low momentum near-wall region deep inside the boundary layer. Mechanical, passive, vane vortex generators, first devised by Taylor and Hoadley[1], are the most common and widely used streamwise fluid vortex generators, and commonly consist of thin solid strips fixed to the surface. However, it has been shown that vane vortex generators impose an increase in drag, caused by both the local pressure increase derived from the flow blockage by the device itself, and by an increase in surface skin friction downstream.

An alternative to vane vortex generators is an active fluid jet vortex-generator, proposed by Wallace[2]. Fluid injection via inclined and skewed (relative to the freestream flow) wall-bounded jets, act to induce longitudinal vortices for flow control, instead of solid vane vortex generators. Air jet vortex generators (AJVGs) usually consist of an array of small orifices, embedded in a surface and supplied by a pressurized air source, wherein longitudinal vortices are induced by the interaction between the jets issuing from each orifice and a freestream fluid flow. The orifices are pitched with respect to the surface tangent and skewed with respect to the freestream flow. Air jet

vortex generators, unlike passive vane vortex generators, do not induce a large increase in drag and they can be actively operated and controlled. Following the work of Wallace, Pearcey [3] undertook a considerable series of experimental studies demonstrating the effectiveness of AJVGs for low and high speed flows. Freestone[4] performed a study of both vane vortex generators and AJVGs (with both circular and rectangular jet orifices) at low speeds and identified that the optimum jet orientation for maximum vorticity generation was a pitch angle (relative to the local surface tangent) of 30^o and a skew angle (relative to the freestream flow vector) of 60^o. With this orientation Freestone showed that the resulting vortex strength could match and, in some cases, exceed that generated by an equivalent vane vortex generator. Many further studies [5]-[11] have been performed over the years into the application of active vortex generating jets for stall suppression. The major detriment, however, to the application of active air jet blowing flow control is its requirement for active energy input – electrical energy for compressing and pumping high pressure air, for example. In addition, the system must be supplied from a source such as the engine where intake air can be bled away to feed the jets. In this case, the system will then result in a small loss in engine efficiency.

This study presents an experimental and computational assessment of a novel passive version of the air jet vortex generator where the internal plenum chamber is removed and the individual upper surface jet orifices connected to the lower surface leading edge by a tube, such that feed air is supplied by ram air induction from the high pressure region in the vicinity of the attachment line.

2 The Experimental Study

Two aerofoil section models were designed and constructed in order to experimentally measure the effect of a passive AJVG system located at 12% chord. The first model employed the NACA 23012C aerofoil section - a modification of the NACA 23012 section, with increased camber and a modified trailing edge to promote trailing edge separation. The model was initially designed with an active AJVG system fed by an internal plenum pipe with compressed air blown in at either end. The model, of chord of 481mm and a span of 740mm, was fitted with a spanwise array of 15 air jets of 4.8mm diameter circular orifices, located at 12% chord and spaced equally apart at 45mm between jet centres. In addition the model was fitted with large end plates to enforce quasi-2D flow and with leading edge sand roughness transition strips. The air jet orifices were designed with 30^o pitch angle and 60^o skew angle to the local aerofoil surface and freestream flow direction.

Once the active blowing experiments were completed, the model was then modified by removing the internal plenum tube, and connecting the upper surface AJVG orifices via a curved 4.8mm diameter steel tube, to contoured intakes at 4% chord on the lower surface. With the limited space available within the leading edge region of the aerofoil, it was not possible to achieve the correct positioning of the intake and exit orifice without a considerable curvature of the duct pipe, that would almost certainly lead to internal flow separation and the generation of considerable swirl. Figure 1 shows the level of duct curvature that was needed to ensure that the intake duct was situated at x/c = 0.05, and the duct exit is at a location x/c = 0.12 for the cases of 30^o skew (computation only) and 60^o skew angle.

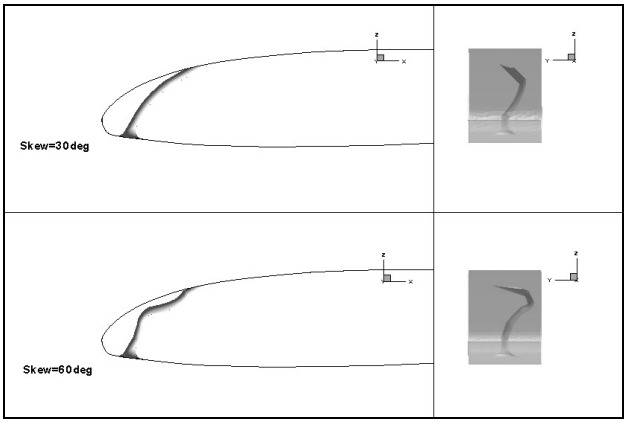

Fig 1: Geometry of a single passive AJVG arrangement, with bent tube ducts installed inside the NACA 23012C aerofoil model section.

A second model, with a greater thickness to chord ratio, incorporating a NACA 63_2-217 section, was constructed with an array of ten passive AJVGs, as shown in figure 2. The model was of span 975mm and 800mm chord, and the AJVGs were located at 12% chord with 84mm spanwise separation between the intake and outlet orifice centres. For this model there was enough space to allow straight ducts as shown in figure 2, such that flow separation and swirl is minimized.

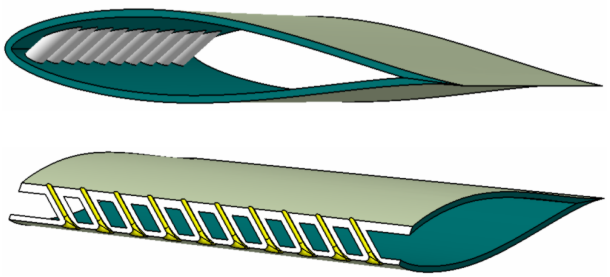

Fig 2: General configuration and cutaway view of the NACA 63_2-217 Aerofoil section model with spanwise array of 10 straight passive AJVGs installed.

Both models were instrumented with three chordwise lines of 82 static pressure orifices each, to allow the measurement of the surface pressure distributions on chordwise planes passing through i) the centre of the orifice located on the centreline of the model, ii) the plane halfway in between this orifice and its adjacent orifice and iii) another plane in the middle of these two. The pressure tappings were constructed from 0.5mm ID brass tube embedded flush with the surface of the model. One of the tappings in each array was located at the trailing edge such that trailing edge pressure could be monitored.

The momentum deficit though the wake one chord length downstream of the trailing edge was measured using a wake rake. The wake rake consisted of 40 stainless steel pitot probes and 5 static probes (OD 1.05mm and ID 0.81mm). The pitot pressure probes were spaced at 7mm intervals in the centre and at 15mm intervals towards each spanwise extremity, giving a total span of 350mm. The static pressure tubes were used to measure any static pressure gradient across the wake. Measuring the pitot and static pressures through the wake, permits the calculation of the drag coefficient using the B.M.Jones expression:

$$C_D = 2\int_{Wake} \sqrt{\frac{p_{01} - p_1}{p_{0\infty} - p_\infty}} \left(1 - \sqrt{\frac{p_{01} - p_\infty}{p_{0\infty} - p_\infty}}\right) d\left(\frac{y}{c}\right) \quad (1)$$

where:
p_{01} = local total pressure (Pa)
p_1 = local static pressure across the wake (Pa)
y = distance normal to the aerofoil wake (m)

A 48 probe shear layer rake was also employed to measure the spanwise distribution of dynamic pressure through the upper surface boundary layer at a number of chordwise planes. The pressures were recorded using a piezosentive pressure measurement system from Chell Systems. Spanwise averaged surface pressure distributions were then used, via an integration routine, to calculate the normal force coefficient (C_N), the axial force coefficient (C_A) and the pitching moment coefficient referenced to the quarter chord axis (C_M).

The NACA23012C experiments were performed in the City University T2 Low speed wind tunnel at speeds in the range 15 – 35m/s ($0.7\text{x}10^6 < Re_C < 1.1\text{x}10^6$), while the NACA 63_2-217 experiments were performed in the City University Industrial wind tunnel in the speed range 5 – 25 m/s ($0.27\text{x}10^6 < Re_C < 1.3\text{x}10^6$). The models were continuously pitched in angle of attack while the working section dynamic pressure was maintained constant. Maximum blockage was estimated at 14%.

3 The Computational Study of the NACA 23012C aerofoil model case

A CFD study was also performed for the case of the NACA23012C model. A commercial 3D time marching Navier-Stokes (N-S) flow solver and grid generation package was used to predict aerodynamic characteristics across the 0-20° angle of attack range. Three turbulence models were tested – the Spalart-Allmaras, and the k-ε and k-ω (SST) turbulence models. In this paper the CFD results for the baseline clean aerofoil are presented across the pitch range,

while for the passive AJVG case only the $\alpha=0^o$ and $\alpha=18^o$ results are presented. The flows for the 30^o and the 60^o skew passive intake-duct-exit air jet geometries were computed for these conditions.

The time-marching flow solver used in this study is based on the finite volume method and can utilize structured, unstructured or hybrid grids. The coupled solver, which simultaneously computes both the continuity, momentum and energy equations, was employed. The solver uses an upwind, flux-difference splitting algorithm and can operate using either implicit or explicit time marching schemes. For the present investigation the spatial accuracy was set to second order.

The geometry and the flow are assumed to be periodically symmetric about any constant-y planes separated by $\Delta y=45mm$ (the spanwise separation between the centres of successive air jet orifices). A computational model was therefore constructed of a 45mm spanwise element that fully encompasses a single air jet intake-duct-orifice, as shown in figure 3. This assumption is valid, based on the published literature, as long as the flow is steady and under prestall condition. A periodic boundary condition can be applied, linking the flow solution on the two constant-y boundaries.

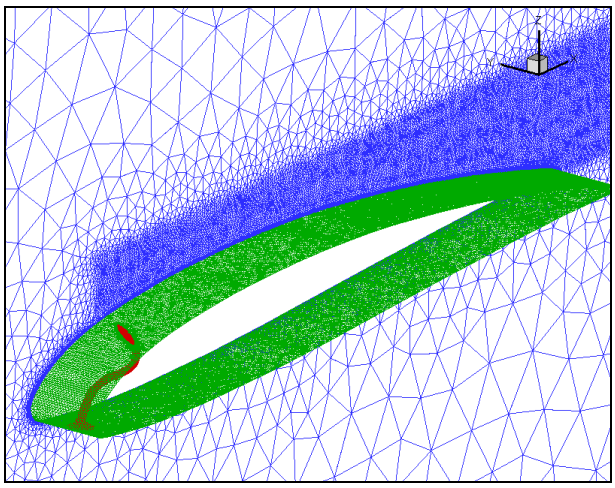

Fig 3: The NACA 23012C 1.7million cell, single element, computational grid for the 60^o skewed jet case. The surface grid is coloured green, the air jet duct red and the y=45mm periodic plane grid appears in blue.

Five computational grids were employed in the study, to ensure grid convergence. A layer of 25 prismatic cells were embedded over the aerofoil surface with the first cell height set at $1x10^{-6}$ chord lengths in order to resolve the boundary layer characteristics with $1.0 < y^+ < 10.0$. The table below presents the grid size details for the 60^o skew passive AJVG predictions.

Grid	Number of cells
1 Coarsest	550,653
2	605,125
3	1,148,223
4	1,675,782
5 Finest	2,161,927

4 Results

4.1 Passive and Active AJVG Blowing on the NACA 23012C Model

The comparisons between the turbulent Navier-Stokes predicted and the experimentally derived variation of the aerodynamic characteristics with angle of attack are presented in figure 4 for the case of U=35m/s.

Figure 5 compares the CFD predicted contours of velocity magnitude through the upper surface boundary layer with the corresponding experimental result at three chordwise locations. The CFD plot was created by plotting the periodically symmetric solution three times. The computed velocity contours at a chordwise plane midway between the between the passive air jet exits (y=0mm =45mm in the computational grid) are presented for $\alpha=18^o$, for the clean aerofoil and both passive AJVG cases, in figure 6. Figure 7 then presents the comparisons of the CFD predicted and experimentally measured surface pressure distributions at the jet-centre and mid-jet spanwise locations, for the $\alpha=18^o$ clean aerofoil and the 60^o skew passive AJVG cases.

The CFD predictions were used to obtain an estimate of how the pressure difference (between the passive AJVG intake and exit) that drives the passive AJVG varies with angle of attack. This variation is plotted in figure 8.

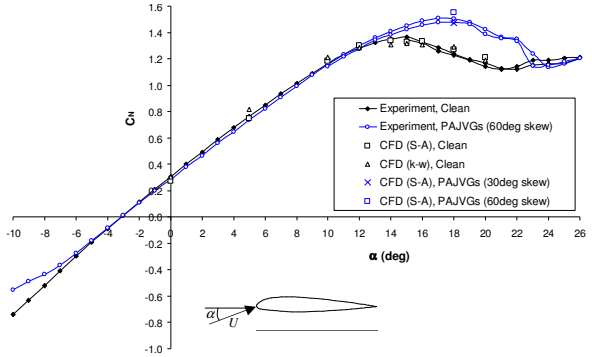

a) C_N versus α.

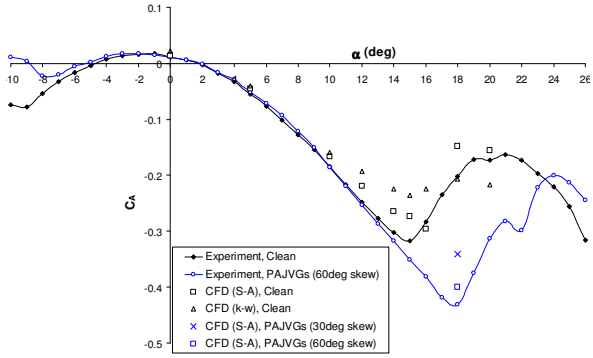

b) C_A (zero skin friction) versus α.

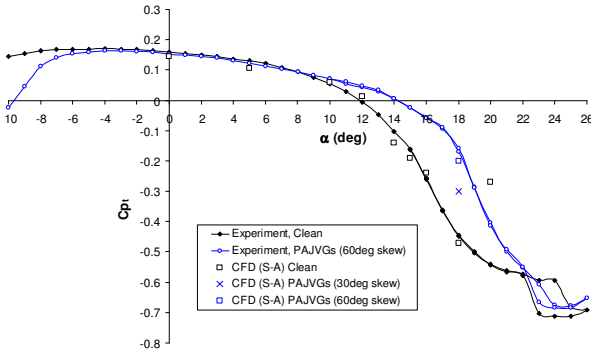

c) Cp_t versus α.

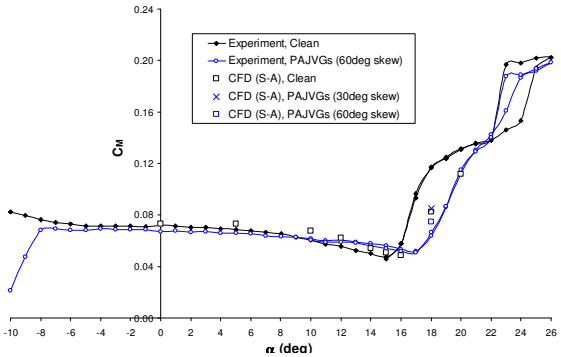

d) C_M versus α.

Fig 4: Comparison of computed (N-S turbulent) and experimental aerodynamic characteristics for NACA 23012C model at U=35m/s.

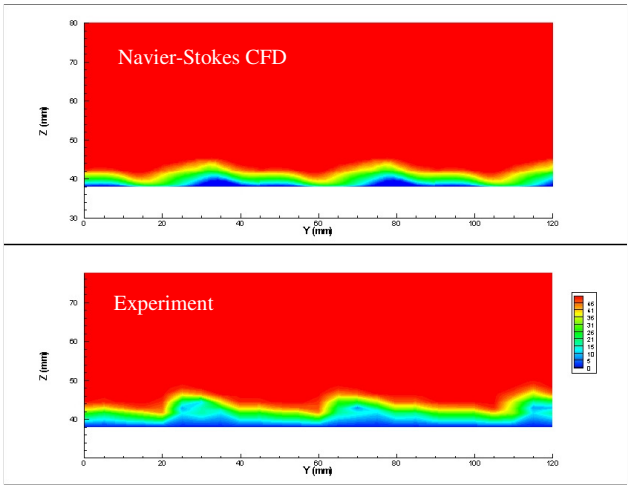

a) x/c=0.2

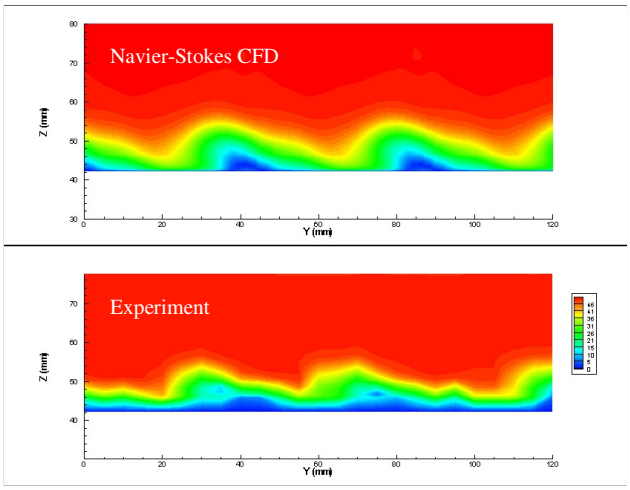

b) x/c=0.3

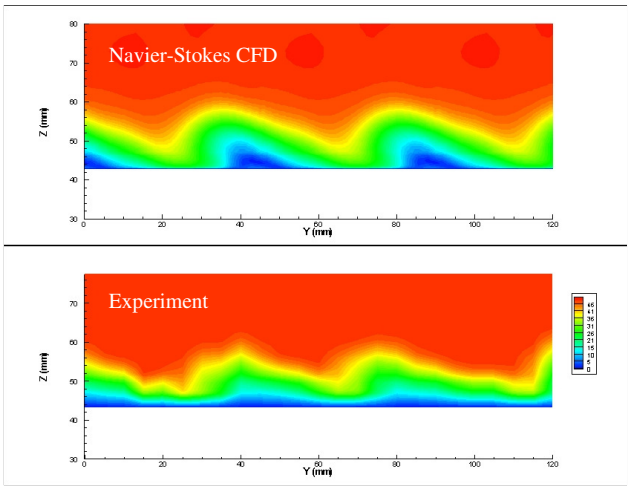

c) x/c=0.4

Fig. 5: Comparison between CFD predicted and experimentally measured velocity magnitude contours in the upper surface boundary layer / embedded longitudinal vortex, at three axial planes along the NACA 23012C model at U=35m/s.

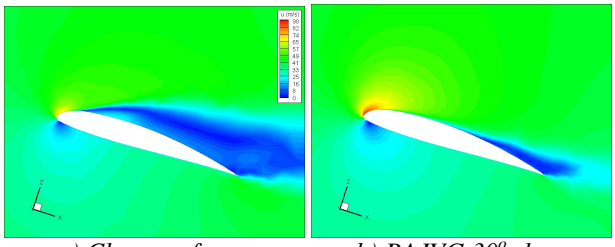

a) Clean surface *b) PAJVG 30^o skew*

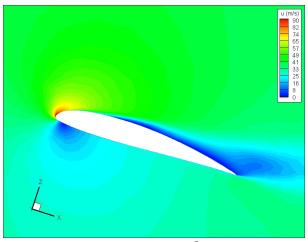

c) PAJVG 60^o skew

Fig 6: Comparison of computed velocity contours at spanwise slice midway between the passive air jet exit centres for the NACA 23012C cases of 30^o and 60^o air jet skew and the corresponding clean aerofoil case. U=35m/s, α=18^o.

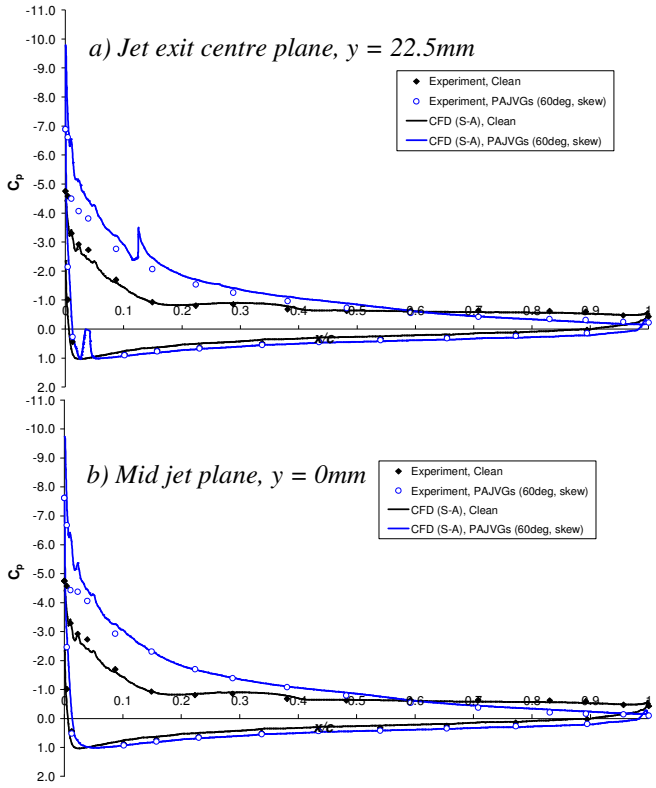

Fig 7: Comparison of experimentally measured and CFD predicted Surface Cp distributions for the NACA 23012C model. U=35m/s, α=18^o.

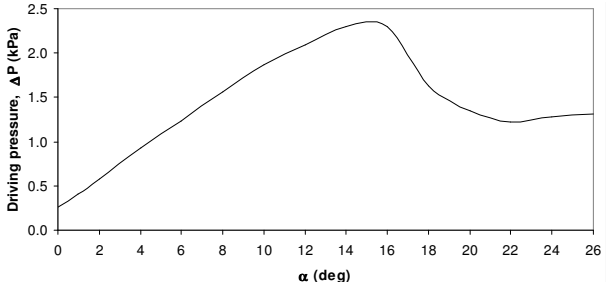

Fig 8: Estimated driving pressure for the passive AJVG system on NACA 23012C model at U=35m/s.

The comparison between the aerodynamic performance of the passive and the active blowing (with C_μ of 0.01) AJVG systems on the NACA23012C are presented in figure 9.

Note that the blowing momentum coefficient is defined as:

$$C_\mu = \frac{\dot{m}U_j}{\frac{1}{2}\rho U_\infty^2 S} \qquad (2)$$

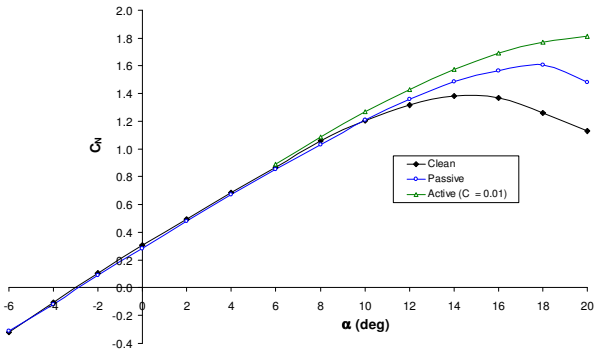

a) C_N versus α

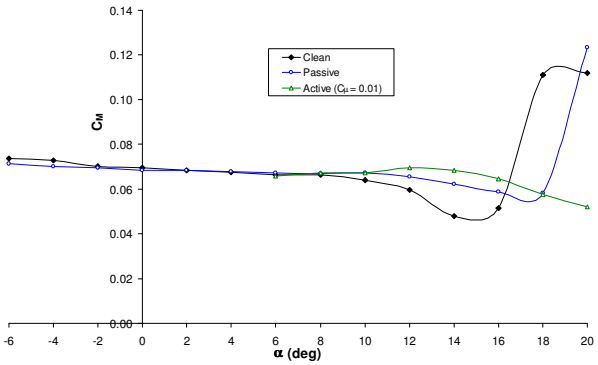

b) C_M versus a

Fig 9: Comparison of the aerodynamic characteristics of the NACA 23012C aerofoil model with active and passive air jet blowing. U=35m/s (continued on next page).

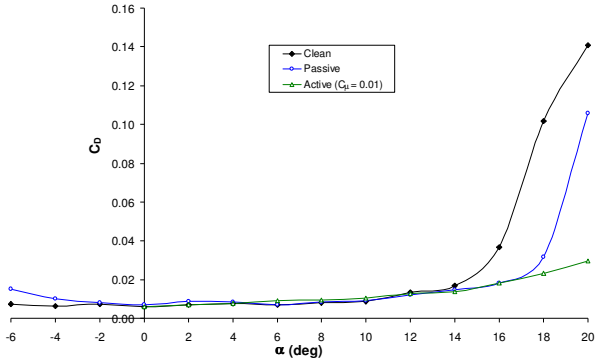

c) C_D versus α

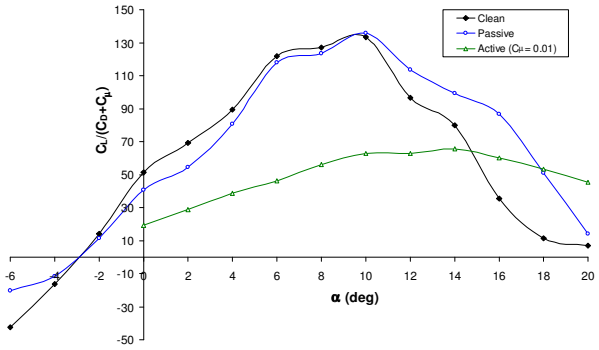

d) $C_L/(C_D+C_\mu)$ versus α

Fig 9: Comparison of the aerodynamic characteristics of the NACA 23012C aerofoil model with active and passive air jet blowing. U=35m/s (concluded).

4.1 Passive AJVG Blowing on the NACA 63_2-217 Model

For the NACA 63_2-217 model no CFD study has yet been performed, and only experimental data was obtained for this thicker aerofoil case. Figure 10 compares the variation of the aerodynamic characteristics with angle of attack for the clean aerofoil and with the 60^o skewed passive air jets operating.

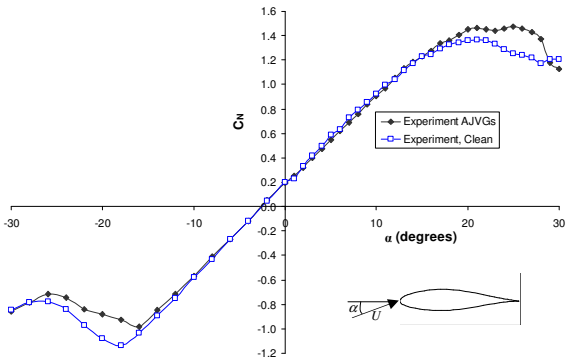

a) C_L versus α

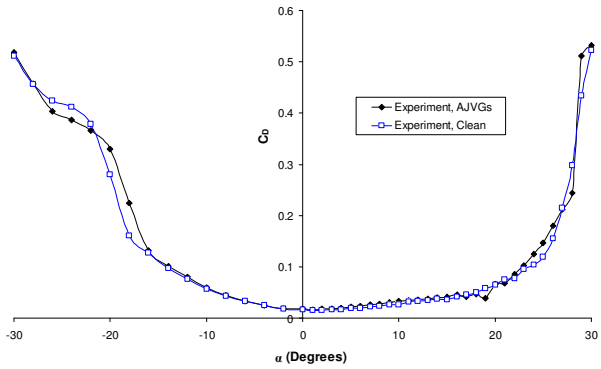

c) C_D versus α

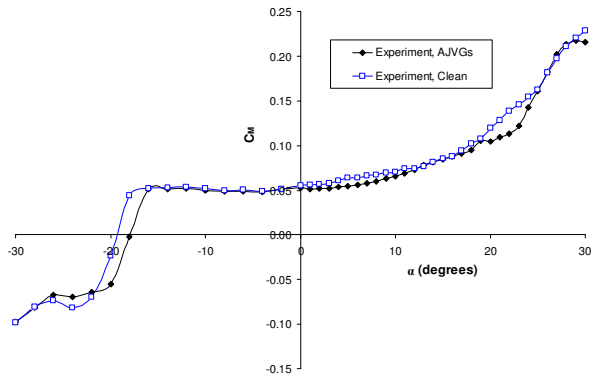

c) C_M versus α

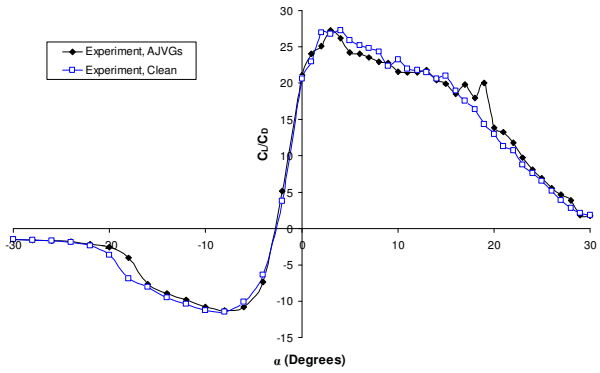

d) C_L/C_D versus α

Fig 10: Comparison of the aerodynamic characteristics of the NACA 63_2-217 aerofoil model with and without passive air jet blowing. U=25m/s.

5 Discussion

5.1 Passive and Active AJVG Blowing on the NACA 23012C Model

Inspection of figure 4 shows that the turbulent N-S solutions for the baseline clean aerofoil model agreed remarkably well with the experimentally derived (integration of surface

pressure) measurements. The CFD solutions successfully resolved the occurrence of trailing edge separation (Cp_t=0) at α~12°, and stall, indicated by C_N and C_A, at α~15-16°. The Spalart-Allmaras predictions resolved the magnitude of C_N to within 3% of the experimental measurement, which itself was estimated to be accurate to within 1% (based on the accuracy of the pressure measurement system and of the pressure integration algorithm). While the agreement between the experimental and predicted axial force coefficients was not as good the turbulent N-S solutions successfully resolved the correct trends. This is as expected since the magnitude of the axial force is much smaller than the normal force, and the pressure integration algorithm more sensitive to numerical error. The Spalart-Allmaras turbulence model was found to predict C_A magnitudes much closer to the experimental values than the k-ω (SST) model. Both turbulence models predicted the pitching moment to within 5% of the experimental values in the prestall angle of attack range.

CFD results for the passive air jet (PAJVG) cases are plotted for α=0° and 18° for the Spalart-Allmaras results only, since these were found to be marginally better than those obtained with the other turbulence models. At α=0° it should be noted that both the experimental measurements and the CFD show that there is no detectable (within the bounds of experimental / numerical accuracy) effect of the passive air jets.

It was originally expected that the significant change in surface geometry caused by the introduction of such a passive jet so close to the leading edge might result in a disturbance of the leading edge suction, and a significant boundary layer displacement effect and thereby drag increase. This, however, does not appear to be the case. While not shown in figure 4, the experimentally measured drag coefficient at low angles of attack (via the B. M. Jones method) was not found to be significantly different with or without the passive air jet. The CFD solutions predicted only a very small (<2%) increase in C_A at low angle of attack.

The passive air jets were found to increase maximum C_N by 14% over that achieved by the baseline model, and to delay the onset of trailing edge separation by Δα~2°. The occurrence of stall, indicated by maximum C_N, was found to be delayed from α=15-16° to α=18-19° by the action of passive air jets, while pitching moment stall was similarly seen to be delayed by Δα~2°. Between α=14-22° passive air jets were found to have significantly increased C_N and negative C_A (indicative of the strength of leading edge suction) with a significantly lower nose up pitching moment. These effects are the same as would be expected of actively blown air jets, operating at the same average C_μ but are achieved by a natural process with no active energy input.

The CFD study indicated (fig. 4) that the passive air jet set at 30° skew angle was not quite as effective as with 60° skew. This agrees with the findings of Freestone [4], though there will almost certainly be a strong effect of the duct geometry inherent in this result.

An experimental survey of the upper surface boundary layer was performed in order to confirm that passive air jets are, indeed, generating the classic boundary layer embedded streamwise vortices, responsible for enhanced boundary layer mixing and reenergisation. Figure 5, comparing the experimental measurements with the corresponding N-S Spalart-Allmaras solutions, shows that the passive air jets, in this U=35m/s, α=18° case, do successfully generate the streamwise vortices. It is also noted that the agreement between the experimental measurements and the CFD prediction is remarkably good at all three chordwise locations, including the spatial location, and structure of the vortices, though they are predicted to be slightly larger and the inner region of the boundary layer is predicted to be signicantly thinner.

Interrogation of the CFD results to reveal the flow structure for the clean aerofoil and the 30° and 60° skew passive air jet cases (fig. 6) reveals that at α=18° the upper surface boundary layer separates at x/c=0.09 without flow control. Only a very small patch (yellow/red) of residual leading edge suction is evident. With passive air jets the separation location, in the mid-jet plane, is seen to be

maintained considerably further downstream in both cases, as well as lengthy regions of strong leading edge suction. The size of the viscous wake is also seen to be considerably reduced by the action of the passive air jets. Comparison of the CFD solutions for the 30° and 60° skew indicate that the spanwise separation line (assuming steady equilibrium) is more "wavy" in appearance for the 60° skew case, than it is with 30° skew.

The comparisons of the surface pressure distributions, for the clean aerofoil at α=18° and with 60° skewed passive air jets, are plotted in figure 7. Again, it can be said that there is a remarkable agreement between experiment and CFD. It should be noted that in the jet-exit centre plane pressure distribution, the spikes in the CFD curve are the surface pressures on the air jet duct surface that intersects this plane. The effect of the passive air jets in maintaining the high levels of leading edge suction is clearly evident in this data.

An important factor in the design of a passive AJVG system is obviously the pressure difference between the air jet contoured intake and exit, which drives the flow through the duct and the attainable jet mass flow and jet to freestream velocity ratio. Figure 8 presents the variation of this driving pressure difference as a function of angle of attack, which was estimated from both the experimental and CFD data for the NACA 23012C model.

The result shows that at α=0° the driving pressure difference is minimal and explains why there does not appear to be any detrimental effects on forces and moments or the pressure distribution at low angle of attack. With increasing angle of attack, up to a maximum at α=15-16°, the driving pressure difference increases almost linearly. This is exactly what is required. At zero to low angles of attack when there is no trailing edge flow separation, air jet blowing is not needed and, in fact, might be detrimental because of the boundary layer displacement effect that might result. As trailing edge separation approaches, however, increasing amounts of air jet blowing are required to reenergize the upper surface boundary layer and suppress flow separation. Strong levels of blowing will also be required once trailing edge separation has occurred, in order to prevent the upstream advance of that separation front and thereby protect leading edge suction. This is exactly the natural behaviour of passive air jet blowing since the driving pressure difference reaches a maximum just after trailing edge separation for the present case of the NACA 23012C model.

This is a major advantage of passive air jet blowing, and the careful designer armed with clean aerofoil pressure data should be able to design a passive AJVG system with natural self flow regulating behaviour, such that minimal blowing occurs at low incidence and maximum blowing occurs around trailing edge separation for the unblown aerofoil.

The comparison between the effect of active blowing at C_μ=0.01 and of passive blowing on the aerodynamic characteristics of the NACA 23012C model at U=35m/s is presented in figure 9 while the table below gives the corresponding estimates of the jet to freestream velocity ratio (*VR*) and C_μ based on both experimental and CFD results.

Air jet blowing	Active	Passive	Passive
Skew angle (deg)	60	30	60
VR	2.50	1.25	1.27
C_μ	0.0100	0.0024	0.0025

While the passive AJVG system, with either skew angle, can only deliver C_μ of up to 0.0025, and *VR* up to ~1.25, the results show that the aerodynamic enhancement, while less than that achieved with C_μ=0.01 active blowing, is still significant and worthwhile. Active blowing delivered a 28% increase in maximum C_N, compared with the passive blowing result of 14%. With passive air jet blowing the pitching moment divergence is seen to be delayed, by 2 degrees, until α=18°, while active blowing is seen to suppress the advent of pitching moment divergence altogether in the range, up to α=20°, investigated. The drag divergence is seen to begin at around α=14°, for the clean aerofoil, 2° above the incipient trailing edge angle of attack. Passive air jet blowing is seen to delay drag rise until between 17 and 18°, 3-4° beyond the onset of trailing edge separation. Active blowing at VR=2.5 (C_μ=0.01), however, was found to

suppress completely the drag rise in the α=0-20^o range. The final plot of figure 9 presents the variation of the *effective* lift to drag coefficient, $C_L/(C_D+C_\mu)$, with angle of attack. The lift to drag ratio for the clean model and the passive air jet cases appear to be equivalent, within the limits of experimental accuracy, up to α=10^o. Beyond this angle of attack the data shows that passive air jet blowing gives increasingly higher lift to drag ratios that the equivalent clean aerofoil case. Since the effective lift to drag ratio includes the effect of air jet blowing momentum coefficient, the data shows that active air jet blowing at C_μ=0.01 gives significantly reduced effective lift to drag ratio performance except at the highest angles of attack. This graph most effectively illustrates the relative efficiency of passive air jet blowing, and the relative inefficiency of active air jet blowing.

5.2 Passive AJVG Blowing on the NACA 63_2-217 Model

The comparison of the *U*=25m/s experimental results for the NACA 63_2-217 model, presented in figure 10 reveals that passive air jets have a similar enhancement effect on the aerodynamic characteristics as on the more slender NACA 23012C model. In this case the passive AJVGs increased maximum C_N by ~9%, while the moment divergence was delayed by $\Delta\alpha$~2-3^o. Within the accuracy of the experimental instrumentation and numerical integration routine, there did not seem to be any appreciable affect of passive air jet blowing on the drag characteristics. There was, therefore, not found to be any significant improvement in *L/D* until above α=16^o, where a maximum 40% increase was measured.

6 Conclusions

This study has confirmed that a spanwise array of passive air jet vortex generators can effectively delay trailing edge separation and subsequent stall to higher angles of attack, thereby increasing maximum C_N, C_L and C_L/C_D, and delaying drag and pitching moment divergence by $\Delta\alpha$=2-3^o, without the need for any active energy input and without significant drag penalty.

References

[1] Talyor D. H, Hoadley H. H, "Application of vortex generator mixing principle to diffusers" Report R-15064-5, United Aircraft corporation, 1948.

[2] Wallis, .R A., "The use of air jets for boundary layer control", Aeronautical Research Laboratories, Australia, Aero. Note no-110, 1952.

[3] Pearcey, H.H., "Shock induced separation and its prevention by design and boundary layer control", Boundary Layer & Flow Control, Ed. G. V. Lachmann, Pergamon Press, pp 1166-1134, 1961.

[4] Freestone, M. "Preliminary tests at low speeds on the vorticity produced by air-jet vortex generators", Research Memo Aero. 85/1, City University, 1985.

[5] Johnston J P, Nishi M, "Vortex generator jets- A means of flow separation control", AIAA Paper 89-0564, 1989.

[6] Compton D. A, Johnston P "Streamwise vortex production by pitched and skewed jets in a turbulent boundary layer" *AIAA Journal*, 30, 3, 1992.

[7] Selby G V, Lin J C, Howard F G, "Control of low speed turbulent separated flow using jet vortex generators", *Experiments in Fluids*, 12, 6,pp.394-400, 1992.

[8] Innes, F., Pearcey, H.H., and Sykes, D.M., "Improvements in the performance of a three element high lift system by the application of air jet vortex generators", *The Aeronautical Journal*, 99, 987, 1995, pp 265-274.

[9] Oliver, A.G., "Air jet vortex generators for wind turbines", PhD Thesis, City University, 1997.

[10] Singh C, Peake, D J, Coton F, Kokkalis A, Khodagolian V, Coton F, Galbraith R A, "Parametric study of an air-jet vortex generator configuration to control rotorcraft retreating blade stall", AIAA Paper 2005-1366, 43rd AIAA Aerospace Sciences Meeting and Exhibit, Reno, Nevada, Jan. 10-13, 2005.

[11] Singh, C., "Application of Air Jet Vortex Generators to Control Helicopter Retreating Blade Stall", PhD Thesis, City University, London 2007.

Acknowledgements

This work was supported and funded by the UK Ministry of Defence, and Department of Trade and Industry as well as Augusta-Westland Ltd., and QinetiQ Ltd.

Copyright Statement